

P. Virtanen and T. T. Heikkilä. 2007. Thermoelectric effects in superconducting proximity structures. *Applied Physics A: Materials Science & Processing*, volume 89, number 3, pages 625-637.

© 2007 Springer Science+Business Media

Reprinted with kind permission of Springer Science and Business Media.

P. VIRTANEN
 T.T. HEIKKILÄ

Thermoelectric effects in superconducting proximity structures

Low Temperature Laboratory, Helsinki University of Technology, P.O. Box 3500, 02015 Helsinki, Finland

Received: 5 February 2007 / Accepted: 14 June 2007
 Published online: 27 July 2007 • © Springer-Verlag 2007

ABSTRACT Attaching a superconductor in good contact with a normal metal gives rise to a proximity effect where the superconducting correlations leak into the normal metal. An additional contact close to the first one makes it possible to carry a supercurrent through the metal. Forcing this supercurrent flow along with an additional quasiparticle current from one or many normal-metal reservoirs leads many interesting effects. The supercurrent can be used to tune the local energy distribution function of the electrons. This mechanism also leads to finite thermoelectric effects even in the presence of electron–hole symmetry. Here we review these effects and discuss to which extent the existing observations of thermoelectric effects in metallic samples can be explained through the use of the dirty limit quasiclassical theory.

PACS 74.25.Fy; 73.23.-b; 74.45.+c; 74.40.+k

1 Introduction

Applying a bias voltage or a temperature gradient across a conductor gives rise to charge and energy currents. The linear response between the biases and currents is described via the thermoelectric matrix, whose diagonal parts are the charge and thermal conductances, and the off-diagonal parts are often referred to as the thermoelectric coefficients. In typical metals, the latter arise due to the asymmetry between positive- and negative-energy excitations with respect to the Fermi energy, i.e., electrons and holes. Such asymmetry in metals is very small, making the typical thermoelectric effects at subkelvin temperatures hard to measure accurately.

Placing a superconductor in good contact with a normal-metal conductor gives rise to finite pair correlations also inside the latter, even when the pair potential inside it vanishes. This superconducting proximity effect has an energy-dependent penetration depth; at typical measurement temperatures on the order of 100 mK it extends up to the micrometer range. The proximity effect modifies the thermoelectric response of the normal conductor. Most importantly, it leads to thermoelectric effects, which are orders of magnitude larger than in the absence of superconductivity. The

proximity-induced modifications are discussed in this paper by employing the quasiclassical theory in the diffusive limit [1–3]. In this theory, we assume that all the relevant length scales of the problem exceed especially the Fermi wavelength (quasiclassical approximation) and the mean free path (diffusive limit). Examples of such relevant length scales are the structure size and the superconducting coherence length. A further property of the quasiclassical theory, especially important for thermoelectric effects, is that it assumes electron–hole symmetry. Because of this, in the normal state it predicts vanishing thermoelectric coefficients.

The proximity modification of the thermoelectric matrix is conveniently described in Andreev interferometers (see Fig. 1), where there are two superconducting contacts to the normal metal. In this structure, the phase difference between the two contacts affects the proximity modifications, and its presence is an important requirement for finite thermoelectric effects, at least within the quasiclassical theory. This type of dependence of the electric conductance on the phase has for example been suggested for use in quantum measurements of flux qubits [4].

This paper is organized as follows. In Sect. 2, we briefly introduce the thermoelectric effects and their relations in normal metals, and then detail the quasiclassical equations for the

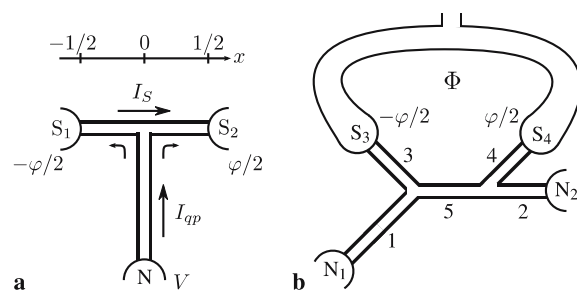


FIGURE 1 (a) Three-probe structure consisting of two superconducting terminals and one normal-metal terminal. The phase difference φ between the superconducting terminals drives supercurrent I_S , and the voltage bias V in the normal terminal drives the quasiparticle current I_{qp} . (b) Andreev interferometer, consisting of a superconducting loop and two normal-metal terminals, connected by five normal-metal wires. The magnetic flux Φ threading the loop controls the superconducting phase difference $\varphi \equiv 2\pi\Phi/\Phi_0$. We take the relative lengths of the wires to be $L_j/L_{SNS} = \frac{2}{3}, \frac{1}{3}, \frac{1}{3}, \frac{1}{3}, \frac{1}{3}$ and assume the wires to have the same cross-sectional area A and conductivity σ . In the numerics, we assume the wires to be quasi-one-dimensional, $\sqrt{A} \ll L$. The absolute size of the system controls the characteristic Thouless energy scale $E_T = \hbar D/L_{SNS}^2$, with $L_{SNS} = L_3 + L_4 + L_5$

diffusive limit. We also discuss briefly effects not addressed in the present paper. Section 3 introduces the properties of the spectral supercurrent and two aspects of nonequilibrium supercurrent. First, we briefly mention the nonequilibrium control of the supercurrent and then concentrate more on how the energy distribution function of electrons is controlled with the supercurrent. The latter is a precursor to the thermoelectric effects. These are described in Sect. 4, which first introduces special symmetries of the thermoelectric matrix, and then details the behavior of its components as a function of the phase difference and temperature. In Sect. 5, we mention the relevant effects when considering the dependence on the magnetic flux, and finally in Sect. 6 we conclude and point out the open questions related to understanding the measurements of the thermoelectric effects.

2 Thermoelectric transport in proximity structures

In this paper, we show that the superconducting proximity effect is able to generate large thermoelectric effects, which can be described without employing the electron–hole asymmetry. An important factor in the theory is the presence of a supercurrent, which then needs to be taken into account in the description of the currents. Moreover, to describe transport between normal metals in the presence of supercurrent, we need to have multiple terminals connected to the structure. As the biases mostly deal with the quasiparticle current, we define the thermoelectric matrix in a multi-terminal structure according to

$$\begin{pmatrix} I_c^i - I_{S,\text{eq}}^i \\ I_E^i \end{pmatrix} = \sum_{j \in \text{terminals}} \begin{pmatrix} L_{11}^{ij} & L_{12}^{ij} \\ L_{21}^{ij} & L_{22}^{ij} \end{pmatrix} \begin{pmatrix} \Delta V_j \\ \Delta T_j / \bar{T} \end{pmatrix}, \quad (1)$$

where I_c^i and $I_{S,\text{eq}}^i$ are the total charge current and the equilibrium supercurrent flowing to terminal i , and I_E^i is the energy current (supercurrent as such carries no energy current). Moreover, ΔV_j is the bias voltage and ΔT_j is the temperature difference from some average temperature \bar{T} , both present in terminal j .

2.1 Transport in normal-metal structures

Thermoelectricity in normal-metal wires can be practically described especially in the diffusive limit (structure size L , elastic mean free path ℓ_{el} and Fermi wavelength λ_F satisfying the relation $L \gg \ell_{\text{el}} \gg \lambda_F$). In this limit, the charge and heat currents flowing in the wire are given by

$$I_c = -eA \int_{-\infty}^{\infty} dE \tilde{D}(E) \nu(E) \partial_x f(x; E) \quad (2a)$$

$$I_Q = -A \int_{-\infty}^{\infty} dE (E - \mu) \tilde{D}(E) \nu(E) \partial_x f(x; E). \quad (2b)$$

Here $\tilde{D}(E)$ is the diffusion constant, $\nu(E)$ is the density of states, A is the cross-sectional area of the wire and x is the coordinate parallel to the wire. The heat current can be simply related to the energy current via $I_Q = I_E - \mu I_c$. For linear

response, $I_Q = I_E$, the second term is responsible for Joule heating, and we can expand the electron energy distribution function $\partial_x f = (\partial_T f) \partial_x T + (\partial_\mu f) \partial_x \mu$, with $f \approx f_0$, the Fermi function. Furthermore, assuming some characteristic length L and taking $\partial_x T = \Delta T/L$ and $\partial_x \mu = e \Delta V/L$ allows us to relate the results to (1).

The energy-dependent changes in the density of states or the diffusion constant typically take place at large energy scales on the order of the Fermi energy E_F . We can thus expand them as $\tilde{D}(E) \approx D + c_D(E - E_F)/E_F$ and $\nu(E) \approx \nu_F + c_N(E - E_F)/E_F$. In first order [of expansion] in c_D and c_N , we find [5]

$$L_{11} = G = e^2 \nu_F D A / L, \quad \text{Drude conductance} \quad (3a)$$

$$L_{22} = L_0 G T^2, \quad \text{Wiedemann–Franz law} \quad (3b)$$

$$L_{12} = e L_0 G' T^2, \quad \text{Mott law} \quad (3c)$$

$$L_{21} = L_{12}, \quad \text{Onsager–Kelvin relation.} \quad (3d)$$

Here $L_0 = \pi^2 k_B^2 / (3e^2) \approx 2.45 \times 10^{-8} \text{ W } \Omega \text{ K}^{-2}$ is the Lorenz number, and the electron–hole asymmetry is described by the factor $G' = e^2 (c_D \nu_F + D c_N) A / (L E_F)$. These relations show that the thermoelectric effects in normal metals are on the order of $k_B T / E_F$.

The Onsager–Kelvin relation between the two thermoelectric coefficients is an example of a more general relation [6–8] between different linear-response coefficients. According to this relation, the elements of the thermoelectric matrix in (1) should satisfy

$$L_{\alpha\beta}^{ij}(B) = L_{\beta\alpha}^{ji}(-B) \quad (4)$$

under the reversal of the magnetic field B . Here $\alpha, \beta \in \{1, 2\}$. This relation results essentially only from the assumption of time-reversal symmetry. In Sect. 4.2, we show how this equation can be derived for the energy-dependent response coefficients within the quasiclassical theory.

The presence of superconductivity modifies the above laws in many different ways [9]. For example, the Andreev reflection [10] breaks the Wiedemann–Franz law, and the Mott law is broken into asymmetric structures [11]. The effects related to the superconducting density of states or to charge imbalance make modifications to the thermoelectric effects at the interfaces [12, 13] and for the nonlinear response [14]. The main modification to linear response due to the proximity effect is the appearance of thermoelectric effects even without electron–hole asymmetry [15–20]. At low temperatures where superconductivity can be observed, the latter effect is much stronger than that expected from the electron–hole asymmetry. Therefore, we concentrate on an electron–hole symmetric theory in the remainder of this paper. We employ the quasiclassical theory that provides a fair description of inhomogeneous superconductivity both in equilibrium and nonequilibrium systems. Moreover, for simplicity and also dictated by many of the experiments, we concentrate on the diffusive limit.

2.2 Usadel equations for proximity structures

Heterostructures composed of diffusive normal-metal or superconducting wires in and out of equilibrium

can be described through the use of Usadel equations [1] for the Keldysh Green's functions \check{G} . These equations are reviewed in many references – we cite here only a few of those [2, 18] applying similar parametrization as here. Written in the Nambu–Keldysh space, the Usadel equation is a nonlinear differential equation for a 4×4 matrix

$$D[\underline{\nabla}, \check{G}[\underline{\nabla}, \check{G}]] = [-iE + \check{\Delta} + \check{\Sigma}, \check{G}]. \quad (5)$$

Here D is the diffusion constant, E is the energy calculated from the Fermi energy, $\check{\Delta}$ denotes the superconducting order parameter and $\check{\Sigma}$ the self-energy for inelastic scattering (mainly the part of electron–electron interaction not described by $\check{\Delta}$ and electron–phonon scattering), for spin-flip or spin-orbit scattering. In the presence of a magnetic field, $\underline{\nabla} \equiv \nabla - ieA\hat{\tau}_3$ is the gauge-invariant derivative including the vector potential A . In addition to (5), \check{G} satisfies the normalization $\check{G}^2 = \check{I}$, where \check{I} is the identity matrix.

In the diffusive limit, we implicitly assume that all the length scales of the problem, including the superconducting coherence length and the mean free paths for other types of scattering than elastic, are much longer than the elastic mean free path. An example of such other types of scattering is the spin-flip scattering, described in the Born approximation by the self-energy [21]

$$\Sigma_{\text{sf}} = \frac{1}{2\tau_{\text{sf}}} \check{\tau}_3 \check{G} \check{\tau}_3, \quad (6)$$

where τ_{sf} is the spin-flip scattering time. This term is included in the following analytic expressions, but omitted from the numerics.

In Keldysh space, Green's function has the form

$$\check{G} = \begin{pmatrix} \hat{G}^R & \hat{G}^K \\ 0 & \hat{G}^A \end{pmatrix},$$

where $\hat{G}^{R/A/K}$ denote the retarded/advanced/Keldysh functions. The latter are 2×2 matrices in the Nambu particle–hole space.¹ Products of this type of matrices yield similar matrices, without mixing the Keldysh parts into the diagonal. Therefore, the Usadel equation (5) also has a similar matrix structure. Employing the normalization and the symmetry $\hat{G}^A = -\hat{\tau}_3 \hat{G}^R \hat{\tau}_3$, we may parametrize

$$\hat{G}^R = \cosh(\theta)\hat{\tau}_3 + \sinh(\theta)(\cos(\chi)i\hat{\tau}_2 + \sin(\chi)i\hat{\tau}_1)$$

and

$$\hat{G}^K = \hat{G}^R(f_L + f_T\hat{\tau}_3) - (f_L + f_T\hat{\tau}_3)\hat{G}^A.$$

Here θ and χ are complex scalar parameters, roughly describing the magnitude and phase of the pair amplitude, respectively. In the Keldysh part, the additional parameters f_L and f_T are the longitudinal and transverse parts of the electron distribution function. It can be shown [21] that this parametrization

spans all the possible solutions of the Keldysh–Usadel equations in nonmagnetic systems.

Usadel equations for θ and χ are

$$D\nabla^2\theta = -2i(E + i\Gamma_{\text{in}}) \sinh\theta + \left(\frac{1}{\tau_{\text{sf}}} + \frac{v_S^2}{2D}\right) \times \sinh(2\theta) + 2i|\Delta| \cos(\phi - \chi) \cosh(\theta), \quad (7a)$$

$$\nabla(-v_S \sinh^2\theta) = -2i|\Delta| \sin(\phi - \chi) \sinh(\theta), \quad (7b)$$

$$v_S \equiv D(\nabla\chi - 2eA/\hbar).$$

Here we assume that the superconducting order parameter is of the form $\Delta = |\Delta|e^{i\phi}$. Note that in a proximity structure, the superfluid velocity v_S is position-dependent. We include the effect of weak inelastic scattering through a constant imaginary part Γ_{in} of the energy [22]. In the numerics, this is set to a small but finite positive value in order to preserve the analytic structure of the Green's functions.

The kinetic equations for the distribution functions read

$$D\nabla\hat{T}_T f = (\nabla j_S) f_L + 2|\Delta|\mathcal{R}f_T, \quad (8a)$$

$$\hat{T}_T f \equiv \mathcal{D}_T \nabla f_T + \mathcal{T} \nabla f_L + j_S f_L,$$

$$D\nabla\hat{T}_L f = 0, \quad (8b)$$

$$\hat{T}_L f \equiv \mathcal{D}_L \nabla f_L - \mathcal{T} \nabla f_T + j_S f_T,$$

where the kinetic coefficients are

$$\mathcal{D}_L = \frac{1}{2}(1 + |\cosh\theta|^2 - |\sinh\theta|^2 \cosh(2\text{Im}[\chi])), \quad (9a)$$

$$\mathcal{D}_T = \frac{1}{2}(1 + |\cosh\theta|^2 + |\sinh\theta|^2 \cosh(2\text{Im}[\chi])), \quad (9b)$$

$$\mathcal{T} = \frac{1}{2}|\sinh\theta|^2 \sinh(2\text{Im}[\chi]), \quad (9c)$$

$$j_S = \text{Im} \left[-\sinh^2(\theta) \frac{v_S}{D} \right], \quad (9d)$$

$$\mathcal{R} = \text{Im} [-\cos(\phi - \chi) \sinh(\theta)]. \quad (9e)$$

Inside a superconductor where the pair interaction parameter $\lambda \neq 0$, the superconducting pair potential is obtained via

$$\Delta = \frac{\lambda}{4} \int dE [(e^{i\chi} \sinh\theta + e^{i\chi^*} \sinh\theta^*) f_L - (e^{i\chi} \sinh\theta - e^{i\chi^*} \sinh\theta^*) f_T]. \quad (10)$$

Solving (7), (8) and (10) we obtain the observables, for example the charge and energy current densities given by

$$J_c = -\frac{\sigma}{2e} \int_{-\infty}^{\infty} dE \hat{T}_T f, \quad J_E = \frac{\sigma}{2e^2} \int_{-\infty}^{\infty} dE E \hat{T}_L f. \quad (11)$$

In most of the text below, we assume that the superconductors are bulky reservoirs, such that the self-consistency equation (10) can be ignored. We rather concentrate on the phenomena taking place in normal-metal wires close to the superconductors. In those wires, we assume $\lambda = 0$, and thereby also $\Delta = 0$. This simplifies the resulting equations.

¹ Throughout the text, we employ the notation where Keldysh matrices \check{A} are checked and Nambu matrices \hat{A} wear a hat. The Pauli matrices in Nambu space are denoted by $\hat{\tau}_i$ and in Keldysh space by $\check{\sigma}_i$, $i = 1, 2, 3$.

2.3 Interfaces and terminals

The Usadel equation holds within the wires where changes in the parameters take place slowly compared to the mean free path. At interfaces, it has to be supplemented by boundary conditions. Initially, these were derived for a general quasiclassical Green's function by Zaitsev [23]. For the diffusive case, the general boundary conditions were solved by Nazarov [24]. They read as

$$\begin{aligned} \check{I}_L = \check{I}_R &= \frac{2e^2}{\pi\hbar} \sum_n \frac{\tau_n [\check{G}_L, \check{G}_R]}{4 - \tau_n (\{\check{G}_L, \check{G}_R\} - 2)}, \\ \check{I}_i &\equiv \sigma_i A_i \check{G}_i \nabla \check{G}_i \hat{n}, \end{aligned} \quad (12)$$

where σ and A are the normal-state conductivity and the cross section of the wires next to the interface, subscript L/R denote left/right from the interface, and \hat{n} is the unit vector perpendicular to the interface, pointing to the right. The interface is characterized by the set $\{\tau_n\}$ of transmission eigenvalues. Note that the resulting expression for \check{I} is linear in the electron distribution functions f , due to the Keldysh block structure of the Green's functions. In what follows, we assume that the normal-state conductance $G_I = 2e^2 \sum_n \tau_n / h$ for each interface is large, such that their effect can be neglected. However, the arguments on the general symmetries of the thermoelectric coefficients are independent of this assumption.

In addition to having the correct boundary conditions for interfaces, one needs also to describe the behavior of the Green's function \check{G} inside different types of terminals. A typical assumption is that the Green's functions obtain their bulk values very close to the interface between a wire and a terminal. Essentially this means that the specific resistance (both charge and thermal) of the terminals should be much smaller than that of the mesoscopic region under study. Experimentally this is realized by especially making the cross section of the normal-metal terminals much larger than that of the wires.

Inside superconductors for energies $E < |\Delta|$ all quantities except f_L relax to their bulk values within distances comparable to the coherence length $\xi_0 = \sqrt{\hbar D / (2\Delta)}$. Moreover, for the L -mode, the Andreev reflection boundary condition $\hat{\Gamma}_L f = 0$ applies at these energies. These details of NS interfaces one can usually describe by increasing the effective length [25] of the normal-metal wires in contact with superconductors by an amount comparable to ξ_0 . However, at energies $E > |\Delta|$, nonequilibrium in f_T and f_L may persist to greater distances. This charge and energy imbalance is limited by inelastic relaxation processes, and for the charge mode in the diffusive limit, by the decoherence induced by a flowing supercurrent or spin-flip scattering (see for example [22, 26]).

For temperatures or voltages on the order or larger than Δ , we hence have to pay some attention to a proper treatment of superconductors, especially superconducting loops (for an example, see Fig. 1) with length L_L , cross section A_L and normal-state conductivity σ_L . Assume such a loop is connected to a normal-metal wire with length L_w , cross section A_w and normal-state conductivity σ_w . When compared to the superconductor, the latter is described by an effective length $L'_w = L_w \sigma_L A_L / (\sigma_w A_w)$ to account for the differences in the

specific resistance. Furthermore, assume an energy relaxation length L_E inside the superconductor. We then have three practically important limits: (a) $L_E \ll L_L, L'_w$, (b) $L'_w \ll L_L \ll L_E$ and (c) $L'_w \ll L_E \ll L_L$. In the first case, the relaxation in the superconductors is fast, and we may assume that $f_L(E > |\Delta|)$ and $f_T(E > |\Delta|)$ acquire their bulk values immediately at the superconducting interface. In case (b), the normal-state resistance of the loop is much higher than that of the normal-metal wires, so that the proper boundary condition is the vanishing of quasiparticle current to the superconductors. For case (c), we again get a vanishing of the quasiparticle charge current, but the energy current will depend on the details of inelastic relaxation in the superconductor.

We see no way to formulate exact mathematical boundary conditions for the limits (b) and (c) above – they in principle require the solution of the Usadel equation inside the superconductor. One attempt to approximate case (b) in a way consistent with the Onsager symmetry is described in Sect. 4.2.1. It captures most of the essential physics of this problem, i.e., taking into account the finite charge and thermal resistance of the loop at high temperatures.

2.4 Unaddressed effects

There are two more practically important self-energies that were not included in the above description: those related to electron–electron and electron–phonon interactions, $\check{\Sigma}_{e-e}$ and $\check{\Sigma}_{e-ph}$. These two have a few distinct characteristics compared to the included scattering mechanisms (mainly elastic and spin-flip scattering):

- They are inelastic scattering mechanisms, i.e., they lead to the nonconservation of spectral currents. This is why these should be taken into account similarly as the self-consistency relation (10). However, electron–electron scattering conserves the total energy and charge current, whereas electron–phonon scattering conserves only the charge current.
- These scattering mechanisms provide both dephasing and energy relaxation, i.e., both their retarded/advanced and Keldysh parts are finite.
- Similarly to the self-consistency relation, these scattering mechanisms make the equations for the retarded/advanced functions depend on the distribution functions f_L and f_T .

The self-energies for these scattering mechanisms in the presence of superconductivity are detailed in [21].

Furthermore, as we concentrate only on the diffusive limit, we neglect effects related to different types of elastic scattering.

3 Supercurrent spectrum and nonequilibrium electron energy distribution function

The presence of the supercurrent-induced terms j_S and \mathcal{T} in (8) leads to the finite thermoelectric effects described in Sect. 4. But before engaging in their discussion, let us look at the spectral supercurrent j_S and how its form can be employed together with a nonequilibrium distribution function to tune the supercurrent flowing in a Josephson junction, or alternatively, to modify the energy distribution function.

3.1 Spectral supercurrent

If a phase-coherent normal-metal wire is sandwiched between two superconductors, Andreev reflection at each NS interface results into a formation of Andreev bound states [27, 28]. In the case of a clean normal metal, these bound-state energies depend on the phase difference φ between the superconducting contacts, the traversal time d/v_F through the normal-metal region of length d , and the transparency τ of the NS interface. For a junction much longer than the superconducting coherence length, the bound-state energies are [29]

$$\varepsilon_n^\pm = \pm \frac{\hbar v_F}{d} \left(\arcsin \sqrt{\tau^2 \cos^2 \left(\frac{\varphi}{2} \right) + (1 - \tau^2) \sin^2(\alpha) + n\pi} \right). \quad (13)$$

Here $\alpha = k_F d + \delta$ is the dynamical phase gathered within traversal through the junction, δ depending on the phase shift at the interface. The characteristic property of these bound states is that they carry an amount of supercurrent proportional to the phase derivative of the bound-state energy. Therefore, we can define a ‘‘spectral supercurrent’’ via

$$j_S \sim \sum_m \frac{\partial \varepsilon_m^\pm}{\partial \varphi} \delta(E - \varepsilon_m).$$

In the clean limit j_S would hence contain a sequence of delta peaks. In the diffusive limit on which we concentrate in this paper, the Andreev state spectrum becomes continuous as disorder gives rise to a distribution of transparencies and times of flights. In this case, j_S can be calculated by solving (7) with proper boundary conditions. Its behavior in different limits is detailed in [30, 31]. An example of $j_S(E)$ specific to the geometries considered in this paper is presented in Fig. 2.

If no dc voltage between the superconductors is applied, the supercurrent between them is obtained from (11)

$$I_S = \frac{\sigma A}{2e} \int_{-\infty}^{\infty} dE f_L(E) j_S(E). \quad (14)$$

Attaching normal-metal terminals to the wire allows one to tune the energy distribution function $f_L(E)$, and thereby the supercurrent [30, 32–34]. Such nonequilibrium supercurrent

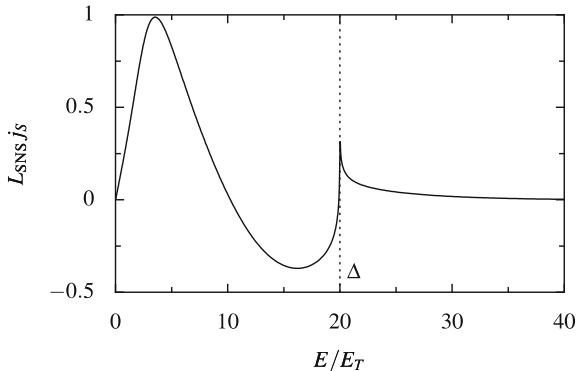


FIGURE 2 Spectrum of the supercurrent in wires 3, 4, 5 in the structure of Fig. 1b, for phase difference $\varphi = 1.6$, and superconducting gap $|\Delta| = 20E_T$

was experimentally demonstrated around the turn of the century by many groups [35–40]. One of the most interesting features of these experiments is the possibility to take the junction into the π -state, where the ground state of the junction corresponds to a phase difference of π between the contacts, and the supercurrent for a given phase difference is reversed compared to the usual 0-state [35, 41]. This π -state occurs when the distribution function f_L weighs the negative part of the supercurrent spectrum more than the positive part (see Fig. 2).

3.2 Driving a nonequilibrium energy distribution with supercurrent

Let us consider the solution to the kinetic equations (8) in a three-probe system depicted in Fig. 1a. The two superconducting terminals are assumed to be at zero potential, whereas the normal-metal terminal is at potential V . For simplicity, let us assume the system is left-right symmetric. In this case, the following symmetries apply inside the horizontal wire

$$\begin{aligned} j_S(\varphi) &= -j_S(-\varphi) \\ \mathcal{T}(\varphi, x) &= -\mathcal{T}(-\varphi, x) = -\mathcal{T}(\varphi, -x) \\ \mathcal{D}_T(\varphi, x) &= \mathcal{D}_T(-\varphi, x) = \mathcal{D}_T(\varphi, -x) \\ \mathcal{D}_L(\varphi, x) &= \mathcal{D}_L(-\varphi, x) = \mathcal{D}_L(\varphi, -x). \end{aligned}$$

In the vertical wire, we hence have $j_S = \mathcal{T} = 0$, and the kinetic equations for f_T and f_L are decoupled. Let us now try to solve for $f_L(x) = f_L^0 + \delta f_L(x)$ in the horizontal wire. Here $f_L^0 = [\tanh((E + eV)/(2k_B T)) - \tanh((E - eV)/(2k_B T))]/2$ is the longitudinal distribution in the normal terminal. Using the fact that for $|E| < |\Delta|$, $\hat{f}_L f = 0$ throughout the normal-metal system, we can find an exact solution for these energies

$$\delta f_L(x) = \int_0^x dx' \frac{\mathcal{T}(x')}{\mathcal{D}_L(x')} (\partial_x f_T)_{x=x'} - j_S \int_0^x dx' \frac{f_T(x')}{\mathcal{D}_L(x')}. \quad (15)$$

This solution can now be substituted into (8a). The latter yields a second order linear differential equation for f_T , independent of f_L . From the full numerical solution we can find that the proximity corrections to f_T are relatively small compared to those in δf_L . Therefore, let us neglect those corrections and solve (8a) in the incoherent limit $\mathcal{D}_T = 1$, $\mathcal{T} = j_S = 0$. In this case we get $f_T(x) = \left(1 - \frac{2|x|}{L_{\text{SNS}}}\right) f_T^c$, where $f_T^c = \varrho_A f_T^0$ is the transverse function at the crossing point $x = 0$. Here $f_T^0 = [\tanh((E + eV)/(2k_B T)) + \tanh((E - eV)/(2k_B T))]/2$ is the boundary condition for f_T in the normal reservoir, $\varrho_A = (\sigma_V A_V L_{\text{SNS}})/(\sigma_V A_V L_{\text{SNS}} + 4\sigma_{\text{SNS}} A_{\text{SNS}} L_V)$, and A_{SNS}/V are the cross sections and σ_{SNS}/V the normal-state conductivities of the horizontal and vertical wires, respectively. Substituting this solution into (15) finally yields

$$\begin{aligned} \delta f_L(x) &= -f_T^0 \varrho_A \\ &\times \left[\frac{2}{L_{\text{SNS}}} \int_0^x dx' \frac{\mathcal{T}(x')}{\mathcal{D}_L(x')} + j_S \int_0^x dx' \frac{1 - \frac{2x'}{L_{\text{SNS}}}}{\mathcal{D}_L(x')} \right]. \end{aligned} \quad (16)$$

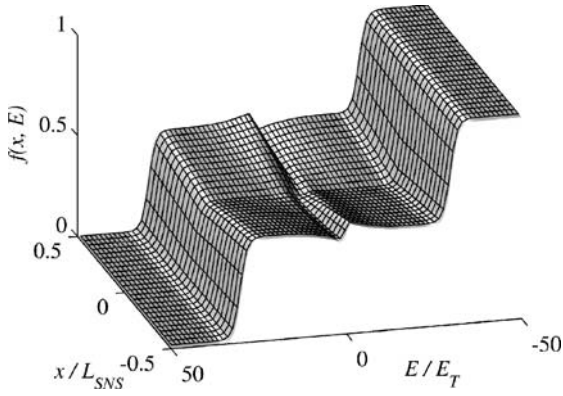


FIGURE 3 Electron distribution function $f(x, E) = \frac{1}{2}[1 - f_T(x, E) - f_L(x, E)]$ between the two superconducting terminals in Fig. 1a. The bias voltage is chosen $V = 30E_T/e$, temperature is $T = 1E_T/k_B$, and $|\Delta| \gg E_T$ and $\varphi = \pi/2$ are assumed. The low-energy ($E \sim E_T$) perturbation in f arises from the L/T mixing in the proximity effect, and the $2V$ -step from the Andreev reflection (see text for more details)

We thus find that the supercurrent controls the antisymmetric part of the distribution function: for a vanishing phase gradient across the wire, $\delta f_L = 0$. For $k_B T \ll eV$, f_T^0 defines a window of energy $E \in [-eV, eV]$ in which the correction is finite (there, $f_T^0 \approx 1$, whereas $f_T^0 \approx 0$ for $|E| > |eV|$). Close to the crossing point $x = 0$, $\mathcal{D}_L \approx 1$, and the energy dependence of $\delta f_L(x)$ reflect directly those of $\mathcal{T}(x)$ and j_S . Close to the NS interface $x \rightarrow \pm \frac{1}{2}$, \mathcal{D}_L tends to zero, and both of the terms in (16) diverge. However, their sum stays finite and the remaining part is roughly proportional to the spectral supercurrent j_S . The full distribution function $f(E, x)$ in the horizontal wire is plotted in Fig. 3 for one example value of the phase difference. The supercurrent-induced changes in the nonequilibrium distribution function were recently measured [42], and the results were in fair agreement with the theory outlined above.

The longitudinal distribution function (the energy mode) f_L describes the response of the electron system to changes in the temperature [26]. In this way, the above changes in f_L can be understood as supercurrent-driven modifications in the local temperature [43]: due to the antisymmetry of $\delta f_L(x)$ about the crossing point $x = 0$, one of the horizontal arms heats up, and another one cools down. Such a setup thus resembles a Peltier-like system. However, in this case one has to deal with an effective temperature T_{eff} (for its definition, see [43, 44]), and it turns out that for this symmetric system the increase in T_{eff} due to the Joule heating is always larger than the changes due to the supercurrent. Both of these issues are settled below when considering the properties of an arbitrarily shaped four-terminal interferometer.

4 Multi-terminal thermoelectric coefficients

In this section, we apply the theory formulated in Sect. 2 to calculate the multi-terminal transport coefficients defined in (1). The main emphasis is on the appearance of thermoelectric effects, which originate from the same mixing of the L- and T-modes that in Fig. 3 modifies the shape of the electron distribution function. Below, we calculate all thermoelectric transport coefficients in the same example setup shown in Fig. 1b, a typical Andreev interferometer. The in-

terference effects due to superconductivity are tuned by the magnetic flux Φ threading the superconducting loop, which adjusts the superconducting phase difference φ , and is observed by measuring various transport properties of the wire between the two normal terminals. We assume here the structure to be left–right asymmetric, as to not miss certain effects that vanish in completely symmetric structures.

4.1 Spectral thermoelectric matrix

Based on the above discussion, one could examine transport in proximity structures simply by solving the Usadel equations numerically and evaluating the current-bias relation for all necessary values of temperatures and voltages at the reservoirs. However, for the proximity effect, it is possible to separate the biases from the full nonlinear response of the circuit by making only mild assumptions.

First, one can note that the only part of the above equations that is nonlinear in the electron distribution functions f is the self-consistency equation (10). Neglecting it is often a good approximation if the terminals are large compared to the rest of the system. Disregarding (10), the linearity in f directly allows one to write the charge and thermal current I_c^i and I_E^i entering a given reservoir i as a linear combination of the distribution functions $f_\alpha^j(E)$ in all reservoirs [20]

$$I_c^i = \int_{-\infty}^{\infty} dE \sum_{\beta j} \tilde{L}_{T\beta}^{ij}(E) f_\beta^j(E), \quad (17a)$$

$$I_E^i = \int_{-\infty}^{\infty} dE E \sum_{\beta j} \tilde{L}_{L\beta}^{ij}(E) f_\beta^j(E). \quad (17b)$$

Similar decomposition has been used in the literature mostly for describing charge transport [45, 46]. Below, we call the set of functions $\tilde{L}_{\alpha\beta}^{ij}(E)$ the spectral thermoelectric matrix, because the thermoelectric linear-response coefficients are related to it in a natural way

$$L_{11}^{ij} = \frac{1}{2k_B T} \int dE \tilde{L}_{TT}^{ij}(E) \text{sech}^2\left(\frac{E}{2k_B T}\right), \quad (18a)$$

$$L_{21}^{ij} = \frac{-1}{2k_B T} \int dE E \tilde{L}_{LT}^{ij}(E) \text{sech}^2\left(\frac{E}{2k_B T}\right), \quad (18b)$$

$$L_{12}^{ij} = \frac{-1}{2k_B T} \int dE E \tilde{L}_{TL}^{ij}(E) \text{sech}^2\left(\frac{E}{2k_B T}\right), \quad (18c)$$

$$L_{22}^{ij} = \frac{1}{2k_B T} \int dE E^2 \tilde{L}_{LL}^{ij}(E) \text{sech}^2\left(\frac{E}{2k_B T}\right). \quad (18d)$$

In principle, the functions $\tilde{L}_{\alpha\beta}^{ij}(E)$ are a generalization of the plain linear-response coefficients.

The matrix element $\tilde{L}_{\alpha\beta}^{ij}(E)$ can be defined explicitly as the α -mode current flowing in terminal i in response to a β -mode unit excitation in terminal j , at energy E

$$\tilde{L}_{\alpha\beta}^{ij}(E) \equiv \int_{\mathcal{S}_i} d\mathcal{S} \hat{n} \cdot \hat{\Gamma}_\alpha \psi^{j,\beta}(E), \quad (19)$$

where \mathcal{S}_i is the surface of the i th terminal and \hat{n} the corresponding normal vector. The two-component characteristic

potential $\psi^{j,\beta} = (\psi_T^{j,\beta}, \psi_L^{j,\beta})$ is assumed to satisfy the kinetic equations together with their boundary conditions, with the distribution function f_α^i in each terminal replaced by $\delta_{\alpha\beta}\delta_{ij}$.

Examples of the energy dependence of the $\tilde{L}_{\alpha\beta}^{ij}(E)$ functions for the four-terminal setup in Fig. 1b are shown in Figs. 4 and 5. The two characteristic energy scales for these coefficients are, similarly as for the spectral supercurrent, the Thouless energy $E_T = \hbar D/L_{\text{SNS}}^2$ and the superconducting energy gap Δ . Note that since our theory is limited to static situations, only L -mode (temperature) bias can be applied to the superconductors if they are at internal equilibrium, for many phenomena, the coefficients in Fig. 4 are more relevant than those

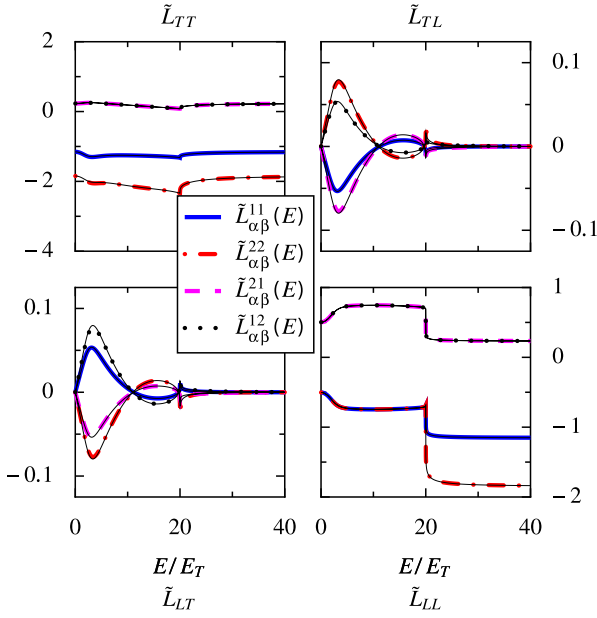


FIGURE 4 Elements of the spectral thermoelectric matrix $\tilde{L}_{\alpha\beta}^{ij}(E)$ associated with the normal terminals, $i, j = 1, 2$, in the structure of Fig. 1b. Phase difference is assumed to be $\varphi = 1.6$ and the superconducting gap $|\Delta| = 20E_T$

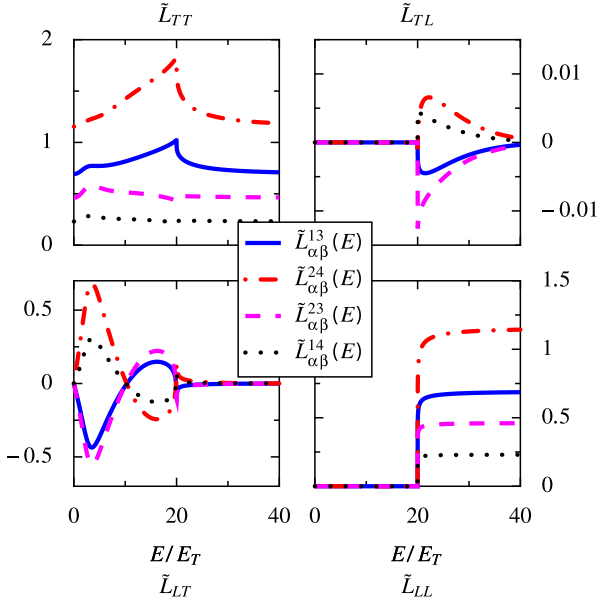


FIGURE 5 Elements of the spectral thermoelectric matrix $\tilde{L}_{\alpha\beta}^{ij}(E)$ associated with excitations in the superconductor, $i = 1, 2, j = 3, 4$. Assumptions are as in Fig. 4

in Fig. 5. However, a nonequilibrium T -mode bias could be generated within the static model by inducing charge imbalance in the superconductors, for example by injecting current from additional normal-metal junctions.

Semi-analytical expressions for the coefficients $\tilde{L}_{\alpha\beta}^{ij}(E)$ can be found by solving (8) up to the first order in j_S and \mathcal{T} . In systems that can be considered as a circuit of quasi-1D wires, this leads to a circuit theory for the distribution functions. Between two nodes with distribution functions $f^1 = (f_T^1, f_L^1)$ and $f^2 = (f_T^2, f_L^2)$, one finds an expression for the spectral currents

$$\hat{\Gamma} f \simeq (\hat{M}^{-1} - ti\hat{\tau}_2 + \frac{\gamma j_S}{2} i\hat{\tau}_2)(f^2 - f^1) + \frac{j_S}{2} \hat{\tau}_1(f^2 + f^1) + \mathcal{O}(j_S^2 + \mathcal{T}^2), \quad (20a)$$

where $\hat{\tau}_1$ and $\hat{\tau}_2$ are Nambu spin matrices, and

$$\hat{M} \equiv \text{diag}(M_T, M_L), \quad M_\alpha \equiv \int_0^L dx \mathcal{D}_\alpha(x)^{-1}, \quad (20b)$$

$$t \equiv \int_0^L dx \mathcal{T}(x) \frac{\mathcal{D}_L(x)^{-1} \mathcal{D}_T(x)^{-1}}{M_L M_T}, \quad (20c)$$

$$\gamma \equiv \int_0^L dx \int_0^L dx' \text{sgn}(x-x') \frac{\mathcal{D}_L(x)^{-1} \mathcal{D}_T(x')^{-1}}{M_L M_T}. \quad (20d)$$

If node 1 (or node 2) is at a clean interface to a bulk superconductor at $E < |\Delta|$, one can use the asymptotic behavior $\mathcal{D}_L(x) = \text{const.} \times x^2 + \mathcal{O}(x^3)$, $\mathcal{T}(x) = j_S x + \mathcal{O}(x^2)$ to find $M_L^{-1} = 0$, $t = 0$, $\gamma = \pm 1$. Using conservation of the spectral current $\hat{\Gamma} f$ at the nodes and suitable boundary conditions, one can in this way find an approximation to $\tilde{L}_{\alpha\beta}^{ij}(E)$ for any given circuit. The quality of this approximation is usually quite good – in Fig. 4 such approximations are shown with black lines, which almost coincide with the numerical results. However, the spectral equations need still to be solved to determine the proximity-modified diffusion constants $D\mathcal{D}_\alpha$, \mathcal{T} and the spectral supercurrent j_S .

4.2 Symmetry relations

As discussed in Sect. 2.1, the normal-state thermoelectric transport coefficients are usually coupled together by Onsager's reciprocal relation $L_{\alpha\beta}^{ij}(B) = L_{\beta\alpha}^{ji}(-B)$ under the reversal of the magnetic field. The question now is: Do the thermoelectric coefficients induced by the proximity effect follow this same relation, and what else can we say about their symmetries. In the framework of scattering theory, it turns out that the Onsager reciprocity applies also in hybrid normal-superconducting systems [9, 47]. Moreover, within the Usadel theory, it has been shown that the off-diagonal coefficients L_{12} , L_{21} are always odd functions of the magnetic field B , whereas the diagonal coefficients L_{11} , L_{12} are even [15, 18, 20]. Below, we review the symmetries present in the Usadel framework.

That a form of Onsager's reciprocal relation applies for the Usadel model can be seen from the structure of the kinetic

equations (8) and symmetries of the coefficients (9) under the reversal of the magnetic fields B (i.e., change of sign in the vector potential A and the superconducting phases ϕ, χ). The crucial observation is that the differential operator $\hat{\mathcal{O}}$ in the kinetic equations (8), $\hat{\mathcal{O}}f = 0$, is related to its operator adjoint by [20]

$$\begin{aligned} \hat{\mathcal{O}}(B)^\dagger &= (-\nabla) \cdot \begin{pmatrix} \mathcal{D}_T & -\mathcal{T} \\ \mathcal{T} & \mathcal{D}_L \end{pmatrix} (-\nabla) + (-\nabla) \cdot j_S \hat{\tau}_1 \\ &\quad - \begin{pmatrix} 2|\Delta|\mathcal{R} & -\nabla j_S \\ 0 & 0 \end{pmatrix} \\ &= \hat{\mathcal{O}}(-B). \end{aligned} \quad (21)$$

Here we exploited the symmetries $\mathcal{D}_\alpha(-B) = \mathcal{D}_\alpha(B)$, $\mathcal{T}(-B) = -\mathcal{T}(B)$, $\mathcal{R}(-B) = \mathcal{R}(B)$, and $j_S(-B) = -j_S(B)$ of the kinetic coefficients (9). From the above relation, it follows that for any two-component functions ϕ, ϱ

$$\int_\Omega dV [\varrho^\dagger \hat{\mathcal{O}}\phi - \phi^\dagger \hat{\mathcal{O}}^\dagger \varrho] = \int_{\partial\Omega} d\mathcal{S} \hat{\mathbf{n}} \cdot J, \quad (22)$$

where the flux $J = \varrho^\dagger \hat{\Gamma}(B)\phi - \phi^\dagger \hat{\Gamma}(-B)\varrho - j_S \varrho^\dagger \hat{\tau}_1 \phi$ is what remains from the integration by parts on the left-hand side. Especially, this flux is conserved when ϕ satisfies the kinetic equations for $+B$, and ϱ for $-B$. Now making use of the functions applied in (19) and substituting $\phi = \psi^{j,\beta}(+B)$, $\varrho = \psi^{i,\alpha}(-B)$, the conservation of J in the volume Ω of the structure implies

$$\begin{aligned} 0 &= \int_\Omega dV [\varrho^\dagger \hat{\mathcal{O}}\phi - \phi^\dagger \hat{\mathcal{O}}^\dagger \varrho] = \int_{\partial\Omega} d\mathcal{S} \hat{\mathbf{n}} \cdot J \\ &= \int_{\mathcal{S}_i} d\mathcal{S} \hat{\mathbf{n}} \cdot \hat{\Gamma}_\alpha(B)\phi - \int_{\mathcal{S}_j} d\mathcal{S} \hat{\mathbf{n}} \cdot \hat{\Gamma}_\beta(-B)\varrho, \end{aligned} \quad (23)$$

when both i and j refer to normal terminals. In this case the last term in J , being proportional to j_S , vanishes on the terminal surfaces \mathcal{S}_i and \mathcal{S}_j . Other terms vanish due to the boundary conditions assumed for the ψ functions. Comparing this result to (19), one finds for i, j referring to the normal terminals

$$\tilde{L}_{\alpha\beta}^{ij}(E, B) = \tilde{L}_{\beta\alpha}^{ji}(E, -B), \quad (24)$$

which is a form of Onsager's reciprocal relation.

A second class of symmetries arises from the way the coefficients $\tilde{L}_{\alpha\beta}^{ij}(E)$ were defined in (17). Namely, we must require that

$$\sum_j \tilde{L}_{LL}^{ij}(E) = 0, \quad (25a)$$

$$\sum_j \tilde{L}_{TL}^{ij}(E) = 0 \quad \text{for normal terminal } i, \quad (25b)$$

so that no net energy current flows to any terminal at equilibrium for any temperature, and that the same applies for the charge current entering the normal terminals.

The third symmetry relation is important for the thermoelectric effects, and is specific to the quasiclassical theory.

Namely, if Green's function \check{G}_1 is a solution to the Usadel equation for vector potential A and self-energy $\check{X}_1[\check{G}_1]$

$$[\nabla - ieA\hat{\tau}_3, \check{G}_1[\nabla - ieA\hat{\tau}_3, \check{G}_1]] = [\check{X}_1[\check{G}_1], \check{G}_1], \quad (26)$$

then, the electron-hole transformed Green's function $\check{G}_2 \equiv -\hat{\tau}_1 \check{G}_1 \hat{\tau}_1$ is a solution to the same equation for $-A$ and self-energy

$$\check{X}_2[\check{G}_2] = -\hat{\tau}_1 \check{X}_1[-\hat{\tau}_1 \check{G}_2 \hat{\tau}_1] \hat{\tau}_1. \quad (27)$$

For $\check{X}_1[\check{G}] = -iE\hat{\tau}_3 + \hat{\Delta}[\check{G}] + \frac{1}{2\tau_{sf}}\hat{\tau}_3\check{G}\hat{\tau}_3$ used above, we note that $\check{X}_2(B) = \check{X}_1(-B)$, where the two functionals coincide. Hence, the transformed Green's function describes the same physical situation, but with an inverted magnetic field. Since electric potentials and charge currents also change sign under this transformation, one finds that [18, 20]

$$\tilde{L}_{\alpha\beta}^{ij}(E, -B) = (-1)^{1-\delta_{\alpha\beta}} \tilde{L}_{\alpha\beta}^{ij}(E, B). \quad (28)$$

This symmetry makes the off-diagonal thermoelectric coefficients odd functions of the applied magnetic field, which is not in agreement with all experiments. We discuss this discrepancy in more detail in Sect. 6 and in the Appendix.

4.2.1 Charge imbalance in superconducting loops. Below, one of the aims is to model qualitative features of charge imbalance in superconducting loops (see Sect. 2.3 and Fig. 1) without solving the Usadel equations inside superconductors. For this, we need some effective boundary conditions to enforce at the NS interfaces instead of the usual terminal assumption (case (a) in Sect. 2.3). Consider a superconducting loop with a large normal-state resistance but long inelastic relaxation length (case (b) in Sect. 2.3). Deep in the superconductor, we then assume that the charge current is carried only as supercurrent with the (BCS) spectral density $j_S \propto \delta(E - |\Delta|)$. Due to the large resistance, we can also assume $\hat{\Gamma}_L\phi = 0$ and $\hat{\Gamma}_T\phi = 0$ for $E \neq |\Delta|$, for any solution ϕ of the kinetic equations. Near the interface, supercurrent conversion occurs and the δ -peak in $\hat{\Gamma}_T\phi$ broadens, which needs to be handled correctly to preserve Onsager reciprocity. Equation (22) defines a flux J that is conserved in the superconductor. By our assumptions, $J = 0$ deep in the superconductor, for $E \neq |\Delta|$. The exact solution f of kinetic equations (8) thus satisfies $J = \psi_T \hat{\Gamma}_T(B)f - f_T \hat{\Gamma}_T(-B)\psi - j_S(\psi_T f_L + f_T \psi_L) = 0$ and $\hat{\Gamma}_L f = 0$ at the NS interfaces of the loop, for any ψ that satisfies $\hat{\mathcal{O}}(-B)\psi = 0$, regardless of boundary conditions.

The only linear boundary condition consistent with the above is $\hat{\Gamma}_T f = G_T(|B|)f_T + j_S f_L$, where G_T describes conductances related to the supercurrent conversion. For simplicity, we then assume $G_T = \infty$ at $E < |\Delta|$ and $G_T = 0$ at $E > |\Delta|$, which results to

$$\Gamma_L f = 0, \quad f_T = 0, \quad E < |\Delta|, \quad (29a)$$

$$\Gamma_L f = 0, \quad \Gamma_T f = j_S f_L, \quad E > |\Delta|. \quad (29b)$$

This acknowledges the fact that for $E < |\Delta|$ the kinetic equations imply a vanishing f_T beyond the current conversion

region, and that in a BCS superconductor f_T does not relax at $E > |\Delta|$ if there is no inelastic scattering [22]. Employing (29) is analogous to requiring that the “nonequilibrium” parts of the spectral currents vanish; the remaining part $j_S f_L$ is what at equilibrium gives rise to the supercurrent.

Note that (29) is not exact: we at least neglect the resistance in the supercurrent conversion region discussed for example in [22, 48]. Note also that when treating a superconducting loop as two boundary conditions, charge conservation must be ensured by adjusting all potentials relative to that of the superconductor. Nonetheless, we expect that (29) captures some of the relevant physics in the problem. Below, we use it to illustrate how charge imbalance could change observable quantities.

4.3 Conductance

How the proximity effect changes the conductance has been studied in detail, both experimentally [47, 49–54] and theoretically [45, 55–57]. For a review, see for example [58].

The modification to conductance can conveniently be described with the Usadel equations. Once $\tilde{L}_{\alpha\beta}^{ij}(E)$ is known – usually the zeroth order in j_S and \mathcal{T} is accurate enough – calculating various conductances can be done. One can directly evaluate the corresponding conductance matrix L_{11}^{ij} and thermoelectric coefficients L_{12}^{ij} from (18) and write

$$dI_c^i = \sum_j L_{11}^{ij} dV_j + \sum_j L_{12}^{ij} dT_j/T + \sum_j \left. \frac{\partial I_c^i}{\partial \varphi_j} \right|_{\{V\}=0, \{\varphi\}} d\varphi_j. \quad (30)$$

The second sum is finite if the heating of the terminals is significant, but should still give only a small contribution as the thermoelectric coupling is small, as can be seen in Fig. 4. The last term arises if conductances are evaluated in structures where the phases φ_j in the superconducting terminals may vary. However, for i referring to a normal terminal, $I_c^i(\{V\}=0, \{\varphi\})=0$ independent of the phases $\{\varphi\}$. This implies that the last term vanishes for conductances around $\{V\}=0$, the potential of the superconductors, but it may be finite when calculating differential conductances. Again, we note also that when modeling superconducting loops using only boundary conditions at the NS interfaces, current conservation needs to be ensured by adjusting all potentials relative to that of the superconducting condensate.

Typical behavior of conductance in an Andreev interferometer is illustrated in Fig. 6. The proximity effect adds an enhancement that oscillates with the superconducting phase difference φ and has a re-entrant dependence on the temperature T . The figure also shows how charge transport via quasiparticles ($E > |\Delta|$) in the superconducting loop may change the conductance at high temperatures. The two curves correspond to the terminal (a) and long-loop (b) limits discussed in Sects. 2.3 and 4.2.1. For the former, the loop contributes to electric conduction at energies $E > |\Delta|$, for the latter it does not.

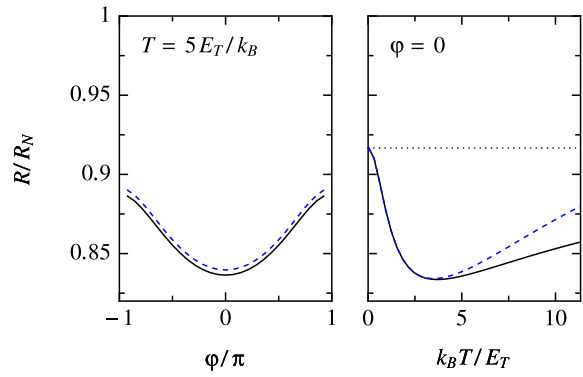


FIGURE 6 Linear-response electrical resistance R between terminals 1 and 2 of the structure in Fig. 1b, as a function of the phase difference φ and the temperature T . The resistances are normalized to the normal-state resistance $R_N = R_1 + R_2 + R_5$. The curves correspond to different models of the superconducting loop discussed in Sects. 2.3 and Sect. 4.2.1, (a) *solid* and (b) *dashed*. The current flows via the superconducting loop as supercurrent, reducing the resistance from the normal-state value also at $T = 0$. Temperature dependence of the energy gap Δ is neglected, and we assume $\Delta = 20E_T$

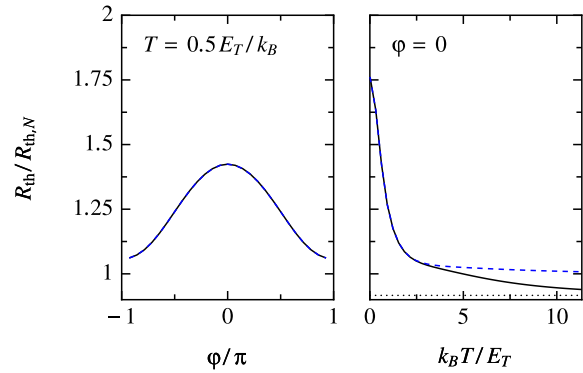


FIGURE 7 As in Fig. 6, but the thermal resistance R_{th} is shown. It is normalized to the normal-state Wiedemann–Franz value $R_{th,N} = 3e^2 R_N / (\pi^2 k_B T)$. The two curves correspond to same models for the superconducting loop as in Fig. 6, (a) terminal (*solid*) and (b) long loop (*dashed*). In the former, at $k_B T \sim \Delta$, part of the thermal current flows through the loop as quasiparticle excitations, reducing the thermal resistance. Note that the scale for R_{th} is the same in both figures

4.4 Thermal conductance

As for the electrical conductance, the proximity of superconductors modifies also the thermal conductance [59–62]. This was studied on the basis of the quasiclassical Usadel theory in [60, 61].

For a given setup, calculation of the thermal conductance from $\tilde{L}_{\alpha\beta}^{ij}(E)$ proceeds as for the electrical conductance. Typical predicted features are φ -periodic suppression of thermal conductance at low temperature $k_B T \lesssim E_T$ due to modified density of states and thermal diffusion coefficient $D\mathcal{D}_L$, and inhibition of subgap thermal transport into the superconductors due to Andreev reflection. These are illustrated in Fig. 7 for the example setup, together with two models for the above-gap quasiparticle transport in the superconducting loop.

4.5 Thermopower

Thermopower S is proportional to the upper right coefficient L_{12} of the thermoelectric matrix. The superconducting proximity effect on S has recently been studied experimentally, (see [63–69]). Theoretically, predictions for

the thermopower in hybrid normal–superconductor structures have been calculated starting from the scattering theory in [9, 11], and via the Usadel theory discussed here [15–19]. We discuss the comparison between theory and the experiment in Sect. 6, and consider here only the theoretical model.

For a two-probe structure, the thermopower is usually defined as the induced voltage divided by the temperature difference when no charge current flows, $S \equiv \frac{dV}{dT} \Big|_{I_c=0}$, but the additional terminals in the four-probe structure in Fig. 1b allow for defining two distinct thermopower-type quantities

$$\begin{aligned} S_{NS} &\equiv \frac{d(V_1 + V_2)}{2d(T_1 - T_2)} \Big|_{I_{c,1}=I_{c,2}=0}, \\ S_{NN} &\equiv \frac{d(V_1 - V_2)}{d(T_1 - T_2)} \Big|_{I_{c,1}=I_{c,2}=0}. \end{aligned} \quad (31a)$$

Both of these can be calculated from $\tilde{L}_{\alpha\beta}^{ij}(E)$

$$S_{NS} = T^{-1} \frac{1}{4} \begin{pmatrix} 1 & 1 \end{pmatrix} \left(L_{11}^{[12]} \right)^{-1} L_{12}^{[12]} \begin{pmatrix} 1 \\ -1 \end{pmatrix}, \quad (32a)$$

$$S_{NN} = T^{-1} \frac{1}{2} \begin{pmatrix} 1 & -1 \end{pmatrix} \left(L_{11}^{[12]} \right)^{-1} L_{12}^{[12]} \begin{pmatrix} 1 \\ -1 \end{pmatrix}, \quad (32b)$$

$$L_{\alpha\beta}^{[12]} \equiv \begin{pmatrix} L_{\alpha\beta}^{11} & L_{\alpha\beta}^{12} \\ L_{\alpha\beta}^{21} & L_{\alpha\beta}^{22} \end{pmatrix}. \quad (32c)$$

Typical results are shown in Figs. 8 and 9. The oscillations in φ are always antisymmetric due to the symmetry relation (28), and the temperature dependence shows the re-entrant behavior on the energy scale of E_T characteristic of the superconducting proximity effect. One can also note that the magnitude of the effect is significantly larger than what is expected from the normal-state thermoelectric effects at subkelvin temperatures, which typically are on the order of $S \approx 10^{-4} \dots 10^{-3} \times k_B/e$.

Making use of expression (20) and neglecting the energy-dependence of \mathcal{D}_T and \mathcal{D}_L one can also derive approximations such as [17]

$$S_{NN} \approx \frac{(R_3 - R_4)R_5^2}{2(R_1 + R_2 + R_5)R_{SNS}} \frac{dI_{S,eq}}{dT} + \frac{R_{SNS}(b_1 + b_2) + (R_3 + R_4)b_5}{(R_1 + R_2 + R_5)R_{SNS}}, \quad (33a)$$

$$S_{NS} \approx \frac{4R_3R_4R_5 + R_5^2(R_3 + R_4)}{4(R_1 + R_2 + R_5)R_{SNS}} \frac{dI_{S,eq}}{dT} + \frac{R_{SNS}(b_1 - b_2) + (R_3 - R_4)b_5}{2(R_1 + R_2 + R_5)R_{SNS}}, \quad (33b)$$

where $R_{SNS} = R_3 + R_4 + R_5$, $|\Delta| \gg E_T$, and

$$b_j \equiv \int_0^\infty \frac{dEE}{2ek_B T^2} \operatorname{sech}^2 \left(\frac{E}{2k_B T} \right) \frac{R_j}{L_j} \int_0^{L_j} dx \mathcal{T}(x) \quad (34)$$

are averages of the coefficient \mathcal{T} in different wires. The approximation (33) is compared to the numerical solution in Figs. 8 and 9. It turns out that a large part of the thermopower is related to the equilibrium supercurrent $I_{S,eq}$ [15, 17]. Note

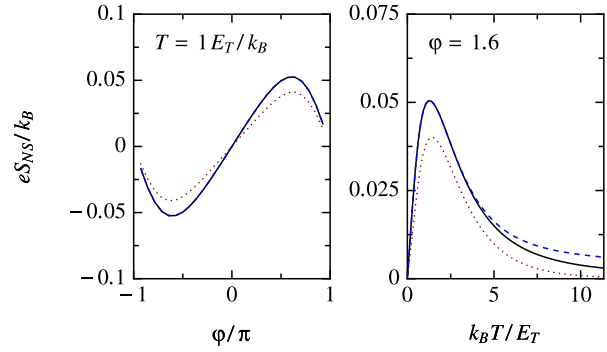


FIGURE 8 Linear-response thermopower in the structure of Fig. 1b, as a function of the phase-difference φ and the temperature T . *Solid line*: no charge imbalance in superconducting loop (case (a) in Sect. 2.3). *Dashed line*: no inelastic relaxation in the long superconducting loop (case (b) in Sect. 2.3). *Dotted line*: approximation (33), neglecting contributions from \mathcal{T} . If the terms proportional to \mathcal{T} are taken into account, the result coincides with the solid line. Other assumptions are as in Fig. 6

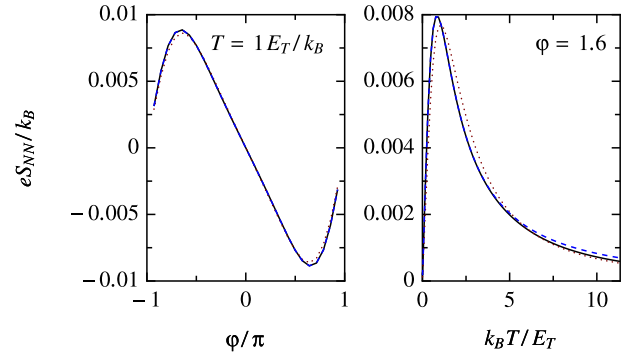


FIGURE 9 As in Fig. 8, but showing the NN thermopower S_{NN} . The *dotted line* includes the terms proportional to \mathcal{T} in (33); the other terms in (33) vanish

also that the contribution from I_S to S_{NN} is strongly dependent on the asymmetry in the structure and vanishes for a left-right symmetric setup, as does the contribution from \mathcal{T} [17, 18]. However, the contribution from energies $E > |\Delta|$, which are neglected here, behaves differently in this respect (see [16, 18, 19]).

4.6 Peltier effect

The second off-diagonal thermoelectric coefficient L_{21} has not yet been measured in the presence of the proximity effect, although related experiments far from equilibrium have been made [42]. Theoretical predictions for modifications due to the proximity effect have been calculated from the scattering theory [9] and from the Usadel theory [20].

A finite L_{21} coefficient induces a Peltier effect, energy current driven by charge current. The Peltier coefficient Π is in general defined as the ratio of the heat current $I_Q = I_E - \mu I_c$ to the charge current at constant temperature, $\Pi \equiv \frac{dI_Q}{dI_c}$. In our example four-probe structure in Fig. 1b, two Peltier coefficients can be defined

$$\begin{aligned} \Pi_{NS} &\equiv \frac{dI_E^1}{dI_c} \Big|_{I_c^1=I_c^2=I_c/2}, \\ \Pi_{NN} &\equiv \frac{dI_E^1}{dI_c} \Big|_{I_c^1=-I_c^2=I_c}, \end{aligned} \quad (35)$$

corresponding to two different current configurations. These are directly related to the linear-response L -coefficients by

$$\Pi_{NS} = \frac{1}{4} \begin{pmatrix} 1 & -1 \end{pmatrix} L_{21}^{[12]} (L_{11}^{[12]})^{-1} \begin{pmatrix} 1 \\ 1 \end{pmatrix}, \quad (36a)$$

$$\Pi_{NN} = \frac{1}{2} \begin{pmatrix} 1 & -1 \end{pmatrix} L_{21}^{[12]} (L_{11}^{[12]})^{-1} \begin{pmatrix} 1 \\ -1 \end{pmatrix}, \quad (36b)$$

in a similar way as in (32). However, note that Π_{NS} can be defined only when there is a grounded extra contact in the superconducting loop (see Fig. 1b) through which the injected current I_c can flow.

As discussed above, the matrix element L_{21} is usually coupled to the element L_{12} via Onsager's reciprocal relation. This leads to Kelvin relations between the Peltier coefficients and the thermopower

$$\Pi_{NS} = TS_{NS}, \quad \Pi_{NN} = TS_{NN}, \quad (37)$$

which are easily seen by transposing equations of (36) and comparing to (32). These relations are not broken by the superconducting proximity effect, which implies that the proximity-induced Peltier coefficient inherits the magnitude, phase oscillations and the temperature dependence of the thermopower. The numerically calculated linear-response Peltier coefficient in the example structure is illustrated in Fig. 10.

The Peltier coefficient is sufficiently large so that it could be detected simply by observing how the effect changes the temperature of one of the terminals in Fig. 1b. For a typical Thouless energy $E_T/k_B = 200$ mK, the coefficient in Fig. 10 achieves a magnitude of $\Pi \sim 1.5$ μ V at temperature $T = 400$ mK. A simple heat balance estimate, assuming that terminal 1 is thermally isolated apart from the electronic heat conduction through wire 1

$$I_Q^1 = -G_{th} \Delta T + 2\Pi_{NS} I_c + eI_c^2/G = 0, \quad (38)$$

then yields a maximum cooling $\Delta T \approx -(3/\pi^2) (e^2 \Pi_{NS}^2 / k_B^2 T) \sim 0.2$ mK. However, the oscillation amplitude is proportional to I_c and can be larger than this maximum cooling effect; variation on the order of millikelvin at least should be possible [20]. Temperature changes of this order have already been successfully resolved in mesoscopic structures [70], so

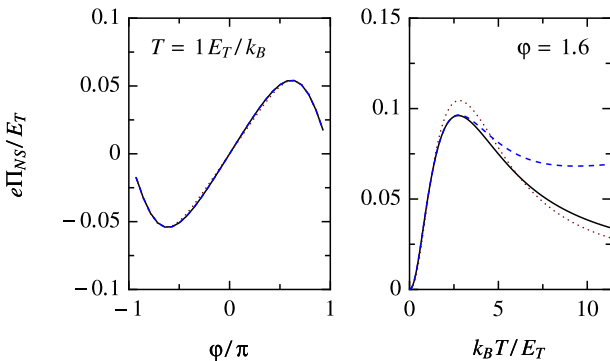


FIGURE 10 As in Fig. 8, but showing the Peltier coefficient Π_{NS} . The dotted line is obtained from the approximation (33) including the \mathcal{T} -terms. The Kelvin relation $\Pi = TS$ can be seen by comparing to Fig. 8

that in a suitably optimized setup, it might also be possible to detect this proximity-Peltier effect.

5 Dependence on external flux

A magnetic field applied to a normal-metal–superconductor heterostructure causes persistent currents to flow in the structure and induces some dephasing. The currents also screen the applied magnetic field, which can usually be taken into account by assigning self-inductances to all loops in the structure. Both effects can be included in the present theory, and we discuss the latter briefly below.

If considering the Andreev interferometer in Fig. 1b, screening is mostly taken into account in the $I_c(\varphi)$ relation of the weak link. The inductance L of the loop only modifies the $\varphi(\Phi_x)$ relation between the induced phase difference φ and the external magnetic field Φ_x to [26, 69]

$$\varphi - 2\pi \frac{\Phi_x}{\Phi_0} = L I_c(\varphi). \quad (39)$$

One should note that although a modified $\varphi(\Phi_x)$ relation should change the shape of the oscillation of various quantities as functions of Φ_x , e.g., thermopower in Fig. 8, the symmetry properties in Sect. 4.2 remain unchanged. However, if there is hysteresis and multiple flux states are possible for the same values of control parameters, the situation is slightly more complicated: for a given solution of (39) with external flux Φ_x , there exists a solution with $-\Phi_x$ for which (24) and (28) apply.

There is a further effect of the magnetic field neglected in this work: the Zeeman effect, which leads effectively to an exchange field inside the wires (for an example of such an effect, see [71]). However, unless special care is taken, this effect plays typically a much smaller role than the dephasing effect of the field.

6 Discussion

In this article, we have systematically discussed the predictions of the quasiclassical diffusive limit theory on the thermoelectric response of normal-metal samples under the influence of the proximity effect. The latter yields corrections to the fairly general relations in (3d). These corrections depend in general on energy (i.e., on temperature or voltage) and on the phase difference between superconducting contacts. At least in most typical cases, one of the general relations, the Onsager relation (and thereby also the Kelvin relation) holds also in the presence of the proximity effect. Furthermore, the approximations made in the quasiclassical theory imply that the diagonal coefficients of the thermoelectric matrix are generally symmetric and the off-diagonal ones antisymmetric with respect to an external magnetic flux.

Our results for the proximity correction of the conductance agree with the previous quasiclassical treatments [45, 55–57]. However, as far as we know, the charge imbalance effect has not been previously addressed. The thermal conductance calculated here is in line with the results in [66], but in contrast to it, we do not make any approximations to the kinetic equations.

The quasiclassical prediction on the thermopower has been detailed in different situations in [15–19]. Our theory is

in line with these predictions. The mechanism for the finite thermopower is analogous to the generation of charge imbalance in bulk superconductors in the presence of coexisting supercurrent and temperature gradient [13, 72–74].

To our knowledge, the only quasiclassical treatment of the Peltier effect and the resulting temperature modification prior to this paper is in our previous work [20]. Beyond the quasiclassical approximation, these effects have been discussed using the scattering theory and numerical simulations of the Bogoliubov–de Gennes equation on a tight-binding lattice [9, 11]. In that work, the symmetry of the flux dependence for the off-diagonal coefficients was mostly dependent on the geometry and disorder of the considered system, and not fixed as in our work. However, the small size of the simulated structures makes a quantitative comparison, for example to the present work, difficult: in [9] even the normal-state thermoelectric effects were large, and it is difficult to distinguish those contributions from the proximity effect that remain large in experimentally relevant structures from those that rely on significant electron–hole asymmetry.

On the experimental side, a qualitative agreement with most of the features presented here has been found. The resistance correction in an Andreev interferometer has been found to oscillate with a magnetic flux through the loop [47, 49–54], with the scale given by the flux quantum. Moreover, the re-entrance effect illustrated in Fig. 6 has been measured in different samples [47, 52, 54]. However, to our knowledge there is no successful quantitative fit between the quasiclassical predictions and the experimentally measured temperature dependence of the resistance (see an example of such a comparison in [54]). The reason for this may be the neglect of the generally temperature-dependent inelastic scattering effects (see Sect. 2.4) in the theory.

The thermopower in the presence of the proximity effect has been measured by two groups, one at Northwestern University, USA [63–66], and another at Royal Holloway University of London [67–69, 75]. Again, most of the qualitative features agree with the quasiclassical theory. The measured thermopower oscillates with the flux and is at least two orders of magnitude larger than the normal-state thermopower, and in line with the predictions from the quasiclassical theory. The first attempt for a quantitative fit [69] of the temperature-dependent thermopower between the theory and the experiments was unsuccessful. We believe that the major reasons for this were the overly complicated geometry of the measurements for this purpose and the neglect of the inelastic scattering effects.

The major qualitative disagreement between the theory and the measurement is in the symmetry of the thermopower oscillations with the flux: in most measurements, the oscillations were antisymmetric and in line with the theory [63–69], in some measurements they were symmetric [65, 66]. The authors of [66] suggested that this symmetry depends on the geometry of the sample: in samples where the supercurrent flows along with the temperature gradient, the oscillations are antisymmetric whereas in other types of samples they are symmetric. Such a conclusion cannot be made based on the quasiclassical theory.

We also note that in bulk superconductors, the magnitude of the thermoelectric effects has been long under debate [76]

– there the experiments have shown larger thermoelectric effects than those predicted by the theory.

The only published measurement on the thermal resistance R_{th} of an Andreev interferometer known to us [62] showed an oscillating R_{th} , but the correction from the proximity effect was larger than that predicted by the theory. We are not aware of any measurements of the Peltier effect.

Quasiclassical theory, based on the combination of the BCS model and the quasiclassical approximation, has been successful in providing a quantitative explanation to a broad range of superconducting phenomena. Here we have pointed out one qualitative aspect (flux symmetry of the thermoelectric effects) which is yet to be explained. Clearly, the full understanding of the nonequilibrium electron transport phenomena in superconducting proximity samples will still require both further experimental and theoretical work.

Appendix: Possible reasons for the symmetric thermopower oscillations

In the diffusive limit, the antisymmetric flux dependence of the proximity-induced thermopower results from the special symmetry of the self-energies: all the typically relevant self-energies satisfy (27) in the presence of a magnetic field B with $\check{X}_2(B) = \check{X}_1(-B)$. Outside the diffusive limit, one has to employ the Eilenberger equation [77] describing the Keldysh Green’s function $\check{g}(\hat{p}, \mathbf{r}, E, B)$. Here \hat{p} is the direction of the electron momentum and \mathbf{r} is the center-of-mass coordinate. In this case, the property of the self-energies $\check{x}[\check{g}]$ leading to the antisymmetric thermopower oscillations is

$$\check{x}[\check{g}(\hat{p}, \mathbf{r}, E, B)] = -\hat{\tau}_1 \check{x}[-\hat{\tau}_1 \check{g}(-\hat{p}, \mathbf{r}, E, -B) \hat{\tau}_1] \hat{\tau}_1. \quad (\text{A.1})$$

This symmetry is satisfied for the most relevant self-energies, including those for the elastic or spin-flip scattering in the Born approximation, and that related to the superconducting order parameter. We note that in [78], it was shown that a dilute concentration of impurities away from the Born limit leads to large thermoelectric effects in unconventional superconductors.

Beyond the quasiclassical approximation, other possible reasons for the symmetric thermopower oscillations may be largely enhanced electron–hole asymmetry effects (however, these were shown in [79, 80] to be small for a fairly generic setup) or quantum interference contributions [81]. Further studies on these effects are therefore required.

ACKNOWLEDGEMENTS This research was supported by the Finnish Cultural Foundation and the Academy of Finland. We thank N. Birge, M. Crosser, M. Meschke and I.A. Sosnin for useful discussions.

REFERENCES

- 1 K.D. Usadel, Phys. Rev. Lett. **25**, 507 (1970)
- 2 W. Belzig, F.K. Wilhelm, C. Bruder, G. Schön, A.D. Zaikin, Superlattices Microstruct. **25**, 1251 (1999)
- 3 V. Chandrasekhar, in *The Physics of Superconductors*, vol. II, ed. by K.H. Bennemann, J.B. Ketterson (Springer, Berlin, Heidelberg, New York, 2004)
- 4 V.T. Petrashov, K.G. Chua, K.M. Marshall, R.S. Shaikhaidarov, J.T. Nicholls, Phys. Rev. Lett. **95**, 147001 (2005)
- 5 M. Cutler, N.F. Mott, Phys. Rev. **181**, 1336 (1969)

- 6 L. Onsager, Phys. Rev. **37**, 405 (1931)
- 7 H.B.G. Casimir, Rev. Mod. Phys. **17**, 343 (1945)
- 8 H.B. Callen, Phys. Rev. **73**, 1349 (1948)
- 9 N.R. Claughton, C.J. Lambert, Phys. Rev. B **53**, 6605 (1996)
- 10 A.F. Andreev, Sov. Phys. J. Exp. Theor. Phys. **19**, 1228 (1964)
- 11 T.T. Heikkilä, M.P. Stenberg, M.M. Salomaa, C.J. Lambert, Physica B **284-288**, 1862 (2000)
- 12 Y.M. Galperin, V.L. Gurevich, V.I. Kozub, A.L. Shelankov, Phys. Rev. B **65**, 64531 (2002)
- 13 A. Schmid, G. Schön, Phys. Rev. Lett. **43**, 793 (1979)
- 14 F. Giazotto, T.T. Heikkilä, A. Luukanen, A. Savin, J. Pekola, Rev. Mod. Phys. **78**, 217 (2006)
- 15 R. Seviour, A.F. Volkov, Phys. Rev. B **62**, 6116 (2000)
- 16 V.R. Kogan, V.V. Pavlovskii, A.F. Volkov, Europhys. Lett. **59**, 875 (2002)
- 17 P. Virtanen, T.T. Heikkilä, Phys. Rev. Lett. **92**, 177004 (2004)
- 18 P. Virtanen, T.T. Heikkilä, J. Low Temp. Phys. **136**, 401 (2004)
- 19 A.F. Volkov, V.V. Pavlovskii, Phys. Rev. B **72**, 14529 (2005)
- 20 P. Virtanen, T.T. Heikkilä, Phys. Rev. B **75**, 104517 (2007)
- 21 N.B. Kopnin, *Theory of Nonequilibrium Superconductivity*, in *International Series of Monographs on Physics* (Oxford University Press, Oxford, 2001), no. 110
- 22 A. Schmid, G. Schön, J. Low Temp. Phys. **20**, 207 (1975)
- 23 A.V. Zaitsev, Sov. Phys. J. Exp. Theor. Phys. **59**, 1015 (1984)
- 24 Y.V. Nazarov, Superlattices Microstruct. **25**, 1221 (1999)
- 25 K.K. Likharev, Rev. Mod. Phys. **51**, 101 (1979)
- 26 M. Tinkham, *Introduction to Superconductivity* (McGraw-Hill, New York, 1996), 2nd edn.
- 27 A.F. Andreev, Sov. Phys. J. Exp. Theor. Phys. **22**, 455 (1966)
- 28 I.O. Kulik, Sov. Phys. J. Exp. Theor. Phys. **30**, 944 (1970)
- 29 N.B. Kopnin, A.S. Mel'nikov, V.M. Vinokur, Phys. Rev. Lett. **96**, 146802 (2006)
- 30 F.K. Wilhelm, G. Schön, A.D. Zaikin, Phys. Rev. Lett. **81**, 1682 (1998)
- 31 T.T. Heikkilä, J. Särkkä, F.K. Wilhelm, Phys. Rev. B **66**, 184513 (2002)
- 32 B.J. van Wees, K.-M.H. Lenssen, C.J.P.M. Harmans, Phys. Rev. B **44**, 470 (1991)
- 33 S.-K. Yip, Phys. Rev. B **58**, 5803 (1998)
- 34 A.F. Volkov, Phys. Rev. Lett. **74**, 4730 (1995)
- 35 J.J.A. Baselmans, A.F. Morpurgo, B.J. van Wees, T.M. Klapwijk, Nature **397**, 43 (1999)
- 36 J.J.A. Baselmans, B.J. van Wees, T.M. Klapwijk, Phys. Rev. B **63**, 094504 (2001)
- 37 J. Huang, F. Pierre, T.T. Heikkilä, F.K. Wilhelm, N.O. Birge, Phys. Rev. B **66**, 020507 (2002)
- 38 T. Schäpers, J. Malindretos, K. Neurohr, S. Lachenmann, A. van der Hart, G. Crecelius, H. Hartdegen, H. Lüth, A.A. Golubov, Appl. Phys. Lett. **73**, 2348 (1998)
- 39 J. Kutchinsky, R. Taboryski, C.B. Sorensen, J. Bindzlev Hansen, P.E. Lindelof, Phys. Rev. Lett. **83**, 4856 (1999)
- 40 R. Shaikhaidarov, A.F. Volkov, H. Takayanagi, V.T. Petrashov, P. Delsing, Phys. Rev. B **62**, R14649 (2000)
- 41 J.J.A. Baselmans, T.T. Heikkilä, B.J. van Wees, T.M. Klapwijk, Phys. Rev. Lett. **89**, 207002 (2002)
- 42 M.S. Cresser, P. Virtanen, T.T. Heikkilä, N.O. Birge, Phys. Rev. Lett. **96**, 167004 (2006)
- 43 T.T. Heikkilä, T. Vänskä, F.K. Wilhelm, Phys. Rev. B **67**, 100502(R) (2003)
- 44 T.T. Heikkilä, Superconducting Proximity Effect in Mesoscopic Metals, Ph.D. thesis, Helsinki University of Technology (2002)
- 45 A.F. Volkov, A.V. Zaitsev, Phys. Rev. B **53**, 9267 (1996)
- 46 H. Courtois, P. Charlat, P. Gandit, D. Mailly, B. Pannetier, J. Low Temp. Phys. **116**, 187 (1999)
- 47 S.G. den Hartog, C.M.A. Kapteyn, B.J. van Wees, T.M. Klapwijk, G. Borghs, Phys. Rev. Lett. **77**, 4954 (1996)
- 48 G.R. Boogaard, A.H. Verbruggen, W. Belzig, T.M. Klapwijk, Phys. Rev. B **69**, 220503 (2004)
- 49 H. Pothier, S. Guéron, D. Esteve, M.H. Devoret, Phys. Rev. Lett. **73**, 2488 (1994)
- 50 P.G.N. de Vegvar, T.A. Fulton, W.H. Mallison, R.E. Miller, Phys. Rev. Lett. **73**, 1416 (1994)
- 51 V.T. Petrashov, V.N. Antonov, P. Delsing, T. Claeson, Phys. Rev. Lett. **74**, 5268 (1995)
- 52 P. Charlat, H. Courtois, P. Gandit, D. Mailly, A.F. Volkov, B. Pannetier, Phys. Rev. Lett. **77**, 4950 (1996)
- 53 H. Courtois, P. Gandit, D. Mailly, B. Pannetier, Phys. Rev. Lett. **76**, 130 (1996)
- 54 W. Belzig, R. Shaikhaidarov, V.V. Petrashov, Y.V. Nazarov, Phys. Rev. B **66**, 220505 (2002)
- 55 Y.V. Nazarov, T.H. Stoof, Phys. Rev. Lett. **76**, 823 (1996)
- 56 T.H. Stoof, Y.V. Nazarov, Phys. Rev. B **53**, 14496 (1996)
- 57 A.A. Golubov, F.K. Wilhelm, A.D. Zaikin, Phys. Rev. B **55**, 1123 (1997)
- 58 C.J. Lambert, R. Raimondi, J. Phys. C Condens. Matter **10**, 901 (1998)
- 59 E. Zhao, T. Löfwander, J.A. Sauls, Phys. Rev. Lett. **91**, 077003 (2003)
- 60 E.V. Bezuglyi, V. Vinokur, Phys. Rev. Lett. **91**, 137002 (2003)
- 61 Z. Jiang, V. Chandrasekhar, Phys. Rev. Lett. **94**, 147002 (2005)
- 62 Z. Jiang, V. Chandrasekhar, Phys. Rev. B **72**, 020502 (2005)
- 63 D.A. Dikin, S. Jung, V. Chandrasekhar, Phys. Rev. B **65**, 12511 (2002)
- 64 D.A. Dikin, S. Jung, V. Chandrasekhar, Europhys. Lett. **57**, 564 (2002)
- 65 J. Eom, C.-J. Chien, V. Chandrasekhar, Phys. Rev. Lett. **81**, 437 (1998)
- 66 Z. Jiang, V. Chandrasekhar, Chin. J. Phys. **43**, 693 (2005)
- 67 A. Parsons, I.A. Sosnin, V.T. Petrashov, Phys. Rev. B **67**, 140502 (2003)
- 68 A. Parsons, I.A. Sosnin, V.T. Petrashov, Physica E **18**, 316 (2003)
- 69 J. Zou, I. Sosnin, P. Virtanen, M. Meschke, V.T. Petrashov, T.T. Heikkilä, J. Low Temp. Phys. **146**, 193 (2007)
- 70 M. Meschke, W. Guichard, J. Pekola, Nature **444**, 187 (2006)
- 71 T.T. Heikkilä, F.K. Wilhelm, G. Schön, Europhys. Lett. **51**, 434 (2000)
- 72 C.J. Pethick, H. Smith, Phys. Rev. Lett. **43**, 640 (1979)
- 73 J. Clarke, B.R. Fjordbøge, P.E. Lindelof, Phys. Rev. Lett. **43**, 642 (1979)
- 74 J. Clarke, M. Tinkham, Phys. Rev. Lett. **44**, 106 (1980)
- 75 G. Srivastava, I. Sosnin, V.T. Petrashov, Phys. Rev. B **72**, 012514 (2005)
- 76 V.L. Ginzburg, Rev. Mod. Phys. **76**, 981 (2004)
- 77 G. Eilenberger, Z. Phys. **214**, 195 (1968)
- 78 T. Löfwander, M. Fogelström, Phys. Rev. B **70**, 024515 (2004)
- 79 F.K. Wilhelm, Ladungstransport in supraleitenden Nanostrukturen, Ph.D. thesis, University of Karlsruhe, Germany (1999)
- 80 B. Meyer, Thermoelektrische Effekte in mesoskopischen Normal-/Supraleiter Heterostrukturen, Master's thesis, University of Karlsruhe, Germany (1999)
- 81 P. Samuelsson, H. Schomerus, Phys. Rev. B **63**, 054512 (2001)